



A green process for zeolite synthesis: low-temperature vapor phase treatment of natural bauxites

Claudia Belviso^{1,*} , Maura Mancinelli², and Antonio Lettino¹

¹Istituto di Metodologie per l'Analisi Ambientale – IMAA-CNR, 85050 Tito Scalo, Potenza, Italy

²Department of Physics and Earth Sciences, University of Ferrara, 44122 Ferrara, Italy

Received: 17 February 2022

Accepted: 3 August 2022

Published online:

3 September 2022

© The Author(s) 2022

ABSTRACT

In this work, three samples of bauxite were used as inexpensive sources for the zeolite formation by a green process based on vapor-phase crystallization (VPC) method. The synthesis was carried out using a water bath with deionized water heated at 35, 45, 60 or 90 °C. During the process, NaOH pre-fused bauxites were contacted only with vapor from the liquid. The results indicate that sodalite formed in all the samples after VPC at higher temperatures (60 °C and 90 °C). Large amount of zeolite A was instead synthesized in the sample characterized by SiO₂/Al₂O₃ ratio next to 1 and after vapor treatment at 35 °C and 45 °C. These data highlight the determining role of both raw material chemical composition and amount of water molecules in type of zeolite formed by vapor crystallization method. Moreover, the results indicate that VPC process made it possible to synthesize zeolite generating no water waste.

Introduction

Bauxites are aluminum deposits formed as results of aluminosilicates rocks weathering under warm, humid, tropical-to-subtropical climate conditions [1–3]. The chemical and mineralogical composition, mainly characterized by the presence of boehmite and kaolinite, makes these rocks as natural sources of Si and Al and therefore as inexpensive raw materials for the zeolite synthesis. Several patents and literature data have in fact documented the zeolite formation by mixtures of bauxite and kaolinite [4–8] whereas Zhang et al. [9] used rice husk together with

bauxite to form FeSAPO-44 by like-dry-gel process. Wang et al. [10] synthesized zeolite X directly from Chinese low-grade bauxite by a two-step synthesis method based on the alkali fusion activation at 350 °C followed by hydrothermal process at 90–100 °C. The use of bauxite to form zeolite was also described by Liu et al. [11]. The authors reported the synthesis of zeolite X adding bauxite to laterite during the hydrothermal process, thus determining the appropriate Si/Al ratio for this type of zeolite formation. Finally, many more papers have documented zeolite synthesis from waste bauxite products (red mud or bauxite tailings) [12–19].

Handling Editor: Christopher Blanford.

Address correspondence to E-mail: claudia.belviso@imaa.cnr.it

Beyond the numerous materials used to synthesize zeolites in addition to aforementioned bauxites [20–26], numerous methods have been employed to synthesize these minerals ranging from conventional hydrothermal to ultrasonic or microwave treatments [27–36]. The processes based on the use of vapor have also been reused in recent years. A distinction on the synthesis processes based on steam was performed by Chen and Huang [37] who, in addition to indicating dry-gel conversion (DGC) as an alternative method to hydrothermal process, explained that “DGC involves treating pre-dried reactive gel powder in water vapor at elevated temperature and pressure. DGC can be further classified into (i) steam-assisted conversion (SAC), where the pre-dried gel powder containing structure directing agent (SDA) is separated from a small amount of pure water in an autoclave which is not in contact with the gel before heating ...and (ii) vapor-phase transport (VPT) in which SDA liquid/solution is placed at the bottom of the autoclave rather than in the initial dry gel powder...”. However, Matsukata and co-workers consider DGC as a generic term for both VPT and SAC techniques [38].

Nishiyama et al. [39, 40] were among the first to perform zeolite synthesis by steam-assisted conversion process (SAC) using non-volatile quaternary ammonium compounds incorporated into dry gel. During the process, only water was supplied from the gas phase. Arnold et al. [41] studied, instead, the conversion of a dry gel into zeolite [Ga] Beta by dry-gel conversion (DGC) process. The authors demonstrated that DGC method determines a breakage and reformation of chemical bonds inside the dry-gel particles, but also a redistribution of the solid particles. The synthesis of ZSM-5 using DGC technique was successfully performed by Mohammadparast et al. [42]. In their paper, the authors showed the formation of nano-zeolites with high crystallinity by initial gel composed of tetrapropylammonium hydroxide (TPAOH), aluminum isopropoxide (Al (O-i-Pr)₃), tetraethylorthosilicate (TEOS), H₂O and NaOH. This gel was dried at different temperatures (100, 115 and 130 °C) before the treatment into autoclave with a small amount of distilled water.

The vapor-phase transport method (VPT) was first developed by Xu et al., 1990 [43] who reported MFI zeolite formation from amorphous dry gel under triethylamine, ethylenediamine and water vapor. Kim et al. [44], demonstrated that an appropriate high pH allows for zeolite synthesis from aluminosilicate gels by contact with vapor of water or

minimal organic reagent and water. The role of water and amines during the crystallization of MFI and FER from dry aluminosilicate gels by VPT method was also analyzed by Matsukata et al. [45], whereas Thoma and Neno [46] studied the relationship between the products of VPT crystallization and both precursor gel and solvent mixtures. The authors concluded highlighting that the amount of water in the VPT solvents represents the determining parameter for the zeolite synthesis, whereas the type of organic molecules has a lower action although it is necessary for the crystallization process. More recently, the transformation of amorphous hollow SiO₂–Al₂O₃ microspheres into microspheres of ZSM-5 by water–organic vapor-phase transport treatment was performed by Cheng et al. [47], whereas Dimitrov et al. [48] published a comparative study of zeolite A crystallization from gel by low hydrothermal method and vapor-phase crystallization process. The results indicated that zeolite crystallites formed by VPT are larger in size (700 nm) compared with the nanocrystals formed by hydrothermal process at 35 °C, 50 °C and 60 °C (50–100, 200 and 300 nm, respectively). According to the authors, zeolite size is controlled by the temperature during the hydrothermal process, whereas the size of starting gel particles involved by vapor treatment determines the larger size of LTA-type nanoparticle zeolite.

In this paper, a process with low environmental impact such as the vapor-phase crystallization (VPC) method was used to form zeolite starting from inexpensive natural raw materials without the addition of pure chemical components or other sources but only exploiting the chemical composition of three different bauxite samples.

Materials and methods

Raw materials and samples characterization

The experiments were performed using three samples of natural bauxite (BAx1, BAx2, BAx3) collected from Upper Cretaceous bauxites exposed in the Murge Plateau of southern Italy [1].

The chemical composition of the bauxite samples (major elements and LOI) was determined by lithium borate fusion—ICP-OES at the Activation Laboratories (Ancaster, Canada).

The mineralogy of raw materials and synthetic products was investigated by X-ray diffraction analysis (XRD) on randomly oriented powders using a Rigaku Rint 2200 powder diffractometer, with Cu K α graphite monochromatized radiation. X-ray diffraction patterns were collected in $\theta - \theta$ geometry, within the angular range of 2–70° of 2θ , step size of 0.02°, scan step time of 3 s and working conditions of 30 kV–40 mA. The GSAS LeBail method with the EXPGUI interface [49] was used to complete the characterization of the samples and determine the peak profiles contribution and the unit cell parameters of the indexed phases. The ratio between crystalline phases (%) was determined by an evaluation using the software DIFFRAC.EVA (Bruker AXS, DIFFRAC. EVA V5.1; Bruker AXS GmbH: Karlsruhe, Germany, 2019). The amorphous material determination was performed on synthetic products using WINFIT computer program [50].

Finally, the morphology and chemical composition of the newly formed zeolites was analyzed by scanning electron microscopy using SEM (Zeiss Supra 40) equipped with energy-dispersive X-ray analysis (EDX; Oxford INCA Energy micro analysis system, x-act Silicon Drift Detector). An estimate of the overall chemical composition of the synthetic products was also determined. Normalized weight percent (wt%) of the elements O, Na, Mg, Al, Si, Ti and Fe was measured. The EDX measurements were taken using accelerating voltage 15 kV, WD = 8.5 mm, aperture \varnothing 30 μ m, measurement time 20 live seconds, magnification \times 10.000. On each sample, four different areas were analyzed. Within each area, a grid of 100 points (10 \times 10) was defined (Fig. S1).

VPC synthesis

The experiments were performed by heating a 1:1.2 bauxite and NaOH weight ratio at 600 °C for 2 h. The resultant fused material was fast cooled and ground with a mortar and pestle for a few minutes. Each sample of pre-fused bauxite was then placed in a ceramic raised holder inside a water bath. The holder was placed in such a way so that the sample inside was contacted only with vapor from the liquid. Figure 1a shows the schematic illustration of set-up experiment hereinafter referred to as *Device #a*.

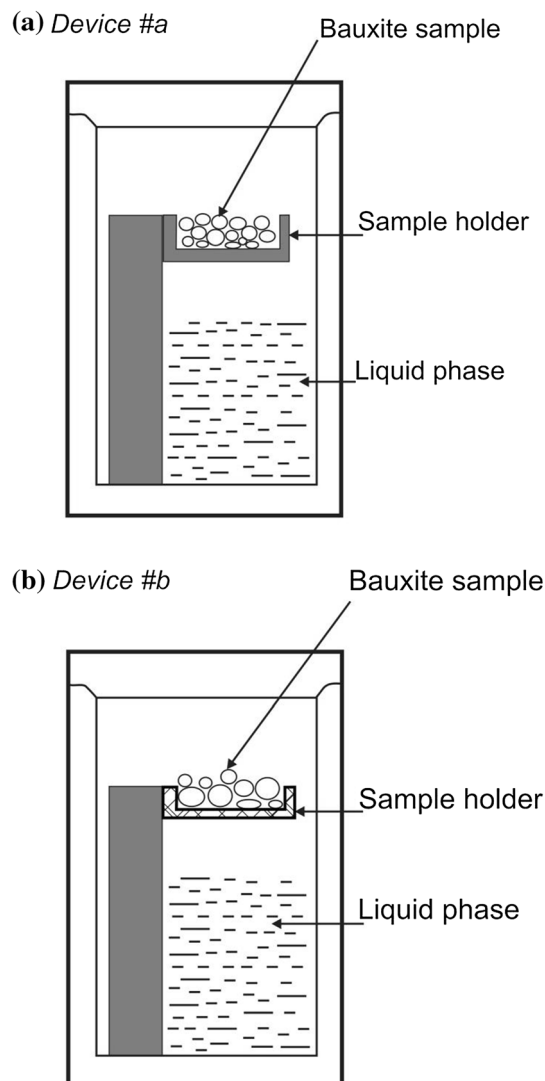


Figure 1 Schematic illustration of water bath with **a** ceramic sample holder (*Device #a*) and **b** sample holder consisting of a metal mesh (*Device #b*) used to form zeolite by a vapor-phase crystallization (VPC) method.

Deionized water was poured into the bottom of water-bath to produce vapor molecules at 35, 45, 60 and 90 °C for 4 days under environmental pressure. The synthetic products were finally dried at 80 °C overnight.

Additional tests were performed on BAX2 using a modified sample holder consisting of a metal mesh of a few millimeters (Fig. 1b—*Device #b*). This new device permits the total immersion of the raw bauxite in the steam without even minimal water accumulation in the sample holder.

Table 1 Raw materials chemical composition (wt %)

Sample	Na ₂ O	MgO	Al ₂ O ₃	SiO ₂	P ₂ O ₅	K ₂ O	CaO	TiO ₂	MnO	Fe ₂ O ₃	LOI	SiO ₂ /Al ₂ O ₃
BAX1	0.05	0.18	41.41	25.95	0.05	0.14	0.49	3.71	0.03	15.22	13.37	0.63
BAX2	0.03	0.11	47.92	15.95	0.02	0.04	0.14	4.17	0.15	19.18	12.58	0.33
BAX3	0.03	0.22	51.80	12.55	0.12	0.16	0.22	4.41	0.05	15.74	14.19	0.24

Results and discussion

Raw materials

The chemical composition of the three bauxites is shown in Table 1. The data indicate that all the samples are characterized by the presence of high percentage of Al₂O₃ estimated equal to 41.41% in BAX1, 47.92% in BAX2 and 51.80% in BAX3. The percentage of SiO₂ is instead 25.95% in BAX1, 15.95% in BAX2 and 12.55% in BAX3. The amount of Fe₂O₃ is highest in BAX2 (19.18%), comparable and just over 15% in the other two samples. The percentage of TiO₂ is also quite high in all the bauxites ranging from 4.41% in BAX3 to 3.71 in BAX1. The amount of Na₂O, MgO and K₂O is low and comparable in all the samples; K₂O lowest value is detected in BAX2 (0.04%). Finally, BAX1 shows the highest amount of CaO (0.49%), whereas MnO is 0.15% in BAX2 and lower in the other two samples (0.03% in BAX1 and 0.05% in BAX3).

Figure 2 XRPD profiles of the three bauxite samples: BAX1, BAX2 and BAX3. *Kln* kaolinite; *Bhm* boehmite; *Hem* hematite; *Gt* goethite; *Ant* anatase.

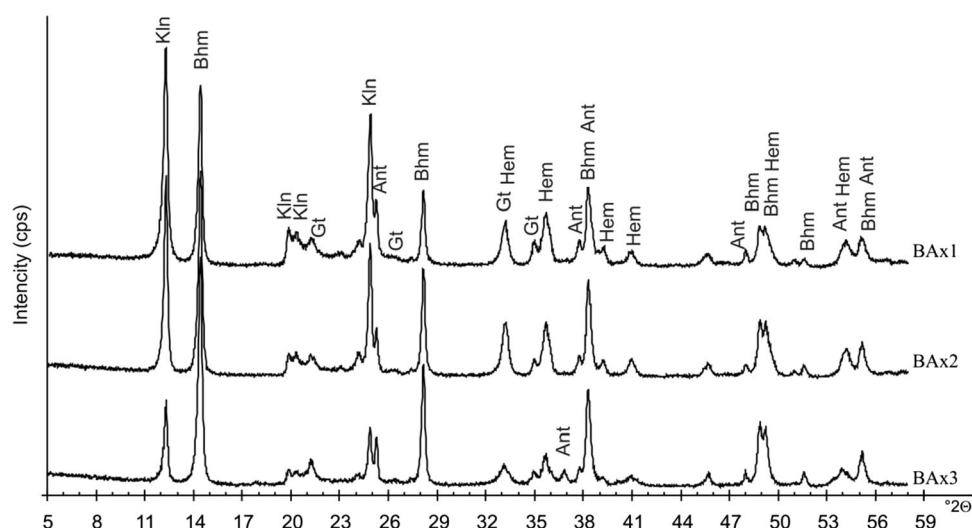


Figure 2 displays the mineralogy of the three natural raw materials. XRD patterns indicate the presence of kaolinite, boehmite, goethite, hematite and anatase. The amount of kaolinite progressively decreases from BAX1 to BAX3, whereas the amount of goethite shows an opposite trend. The peaks of boehmite are higher in BAX3 compared to BAX2; they are lowest in BAX1.

Based on the chemical and mineralogical results, the samples of bauxite analyzed are suitable as sources for zeolite synthesis.

Synthetic products

The results display that zeolite formed in all the samples. Trace of precipitated non-zeolite phases or relict phases from raw materials are also detectable. Figure S2 shows X-ray powder diffraction patterns for refined synthetic products. Tables S1–S4 display the percentage evaluation of the main zeolite phase as well as the estimate chemical composition of all the synthetic samples.

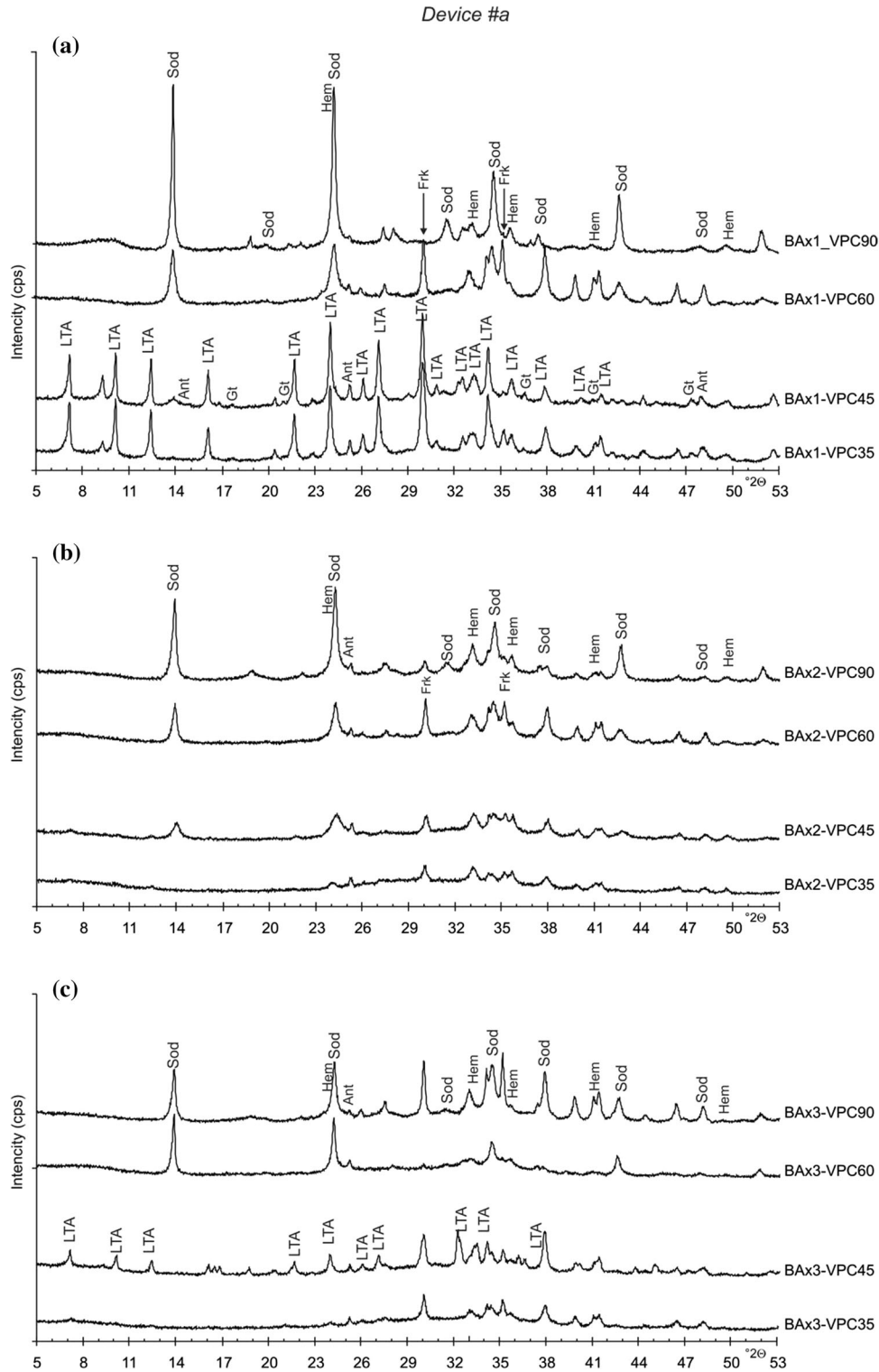


Figure 3 XRD patterns of: **a** BAX1; **b** BAX2 and **c** BAX3 after vapor-phase crystallization (VPC) process at different temperatures using Device #a. LTA zeolite A; Sod sodalite; Frk franklinite; Hem hematite; Gt goethite; Ant anatase.

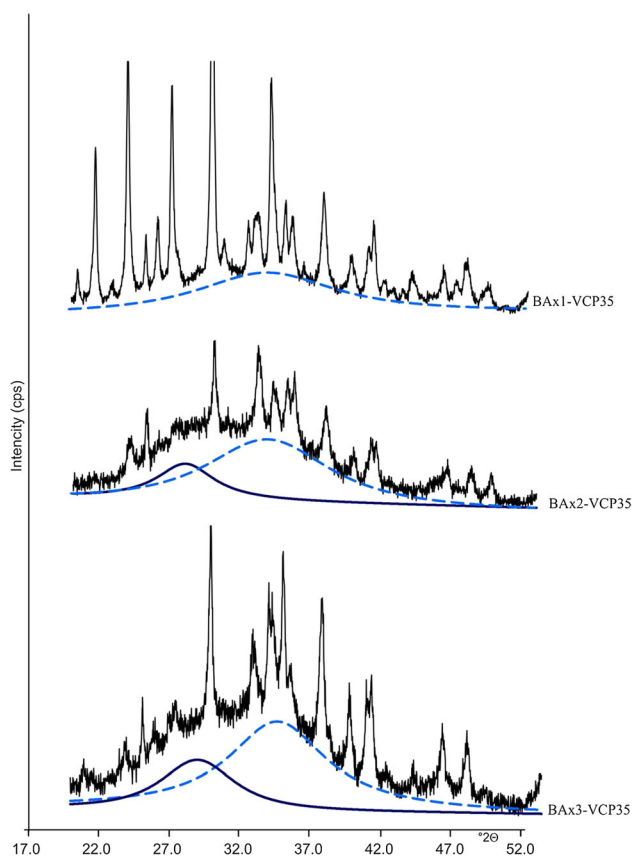


Figure 4 Detail of XRD patterns of bauxite samples after VPC treatment at 35 °C using *Device #a*. Full line = geopolymer material; dashed line = glass amorphous material.

XRD profiles in Fig. 3 indicate that BAX1 sample after VPC process at 35 °C using *Device #a* is characterized by the presence of zeolite with LTA topology (zeolite A) (Fig. 3a). The newly formed phase is weakly detectable on XRD patterns of the other two samples (Fig. 3b, c). These results can be explained considering that the lower amount of water molecules produced by steam treatment at 35 °C determines a weak dissolution of Na silicate-aluminosilicate phases in all the pre-fused bauxite samples. The following formation of geopolymer and/or glass amorphous material controls the synthesis of zeolite. The mechanism takes place essentially through a solid-state transformation process of geopolymers into well-defined crystals.

Detailed XRD pattern in Fig. 4 indicates that BAX1-VCP35 is characterized by the presence of geopolymer amorphous material, whereas the chemical data in Table 1 display that $\text{SiO}_2/\text{Al}_2\text{O}_3$ ratio of BAX1 is 0.63. This means that chemical composition of the geopolymers formed at the first stage of

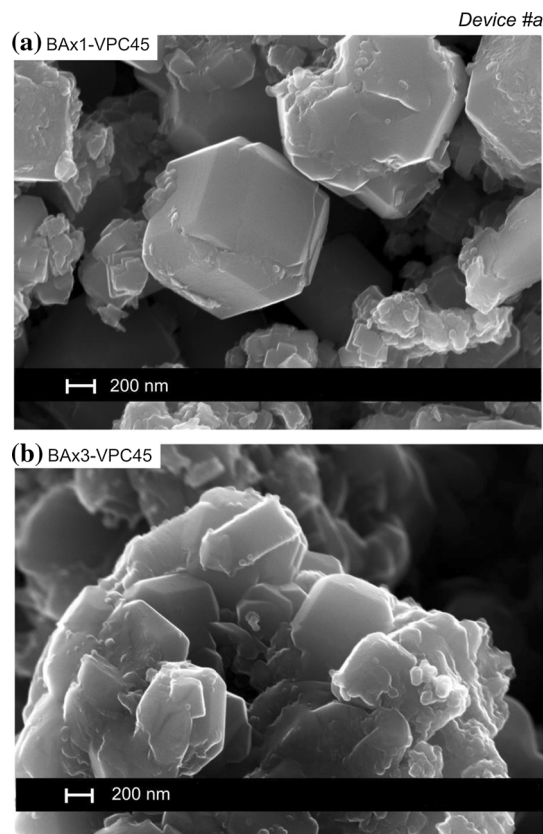


Figure 5 SEM images of: **a** BAX1 and **b** BAX3 after VPC process at 45 °C using *Device #a*.

crystallization mechanism is close to the stoichiometric LTA composition [27], thus explaining the higher amount of newly formed zeolite A in BAX1-VCP35 sample (Fig. 3a). BAX2-VCP35, instead, shows the additional presence of amorphous glass together with geopolymers, as indicated by second broad band shifted to lowest angles (Fig. 4). These two bands attributable to amorphous materials with different initial crystalline order [51–53] are also detectable on BAX3-VCP35 profile (Fig. 4). The presence of non-reactive amorphous material (amorphous glass) limits the formation of zeolite, thus explaining the absence of this newly formed mineral in both BAX2VCP35 and BAX3VCP35C (Fig. 3). Moreover, the chemical data in Table 1 show $\text{SiO}_2/\text{Al}_2\text{O}_3$ ratio much less than 1 for both BAX2 and BAX3 samples.

After VPC process at 45 °C, zeolite A is abundant in BAX1-VPC45 (Fig. 3a), weakly detectable in BAX2-VPC45 (Fig. 3b) and present in BAX3-VPC45 but in less quantity compared to BAX1-VPC45 (Fig. 3c). SEM images in Fig. 5 confirm the presence of well-

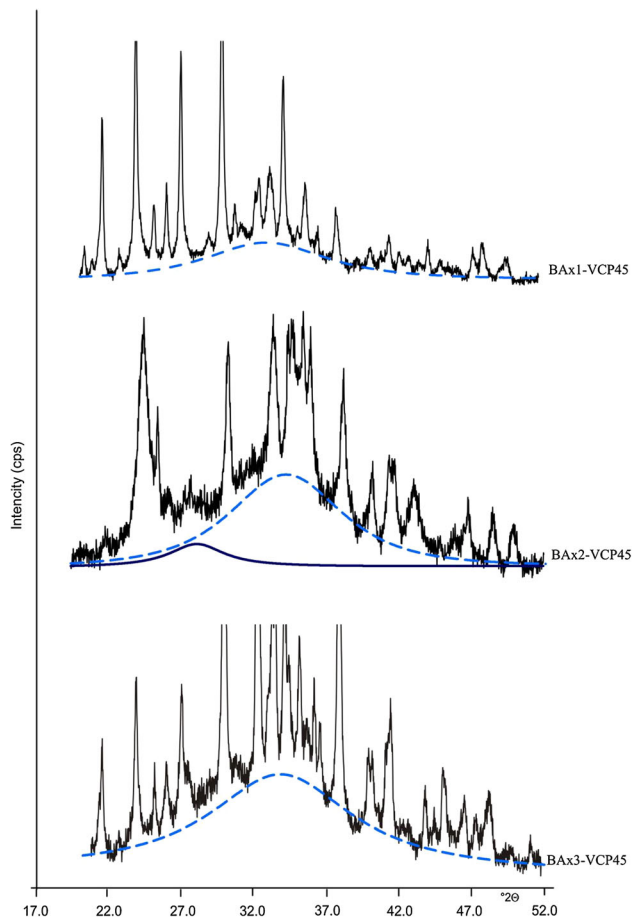


Figure 6 Detail of XRD patterns of bauxite samples after VPC treatment at 45 °C using *Device #a*. Full line = geopolymer material; dashed line = glass amorphous material.

defined cubic LTA morphology in BAx1-VPC45 and BAx3-VPC45. EDX data of the newly formed zeolite are shown in Fig. S3. The crystallization of larger amount of zeolite with LTA topology is generally due to the higher concentration of water molecules in the system, according to the higher temperature, thus determining a larger amount of geopolymers evolving into well crystalline structure. This is confirmed by the presence of a broad band made up of geopolymers in both BAx1-VPC45 and BAx3-VPC45 patterns (Fig. 6). However, Fig. 6 shows that geopolymer broad band in BAx1-VPC45 is comparable with the amount of this amorphous phase detected in BAx1-VPC35 (Fig. 4) and this is in agreement with the same amount of zeolite A analyzed in both XRD pattern shown in Fig. 3a. Figure 6, instead, indicates that BAx3-VPC45 is characterized by the only presence of geopolymer, whereas BAx3-VPC35 displays the presence of amorphous glass

(Fig. 4). The geopolymerization of no reactive amorphous phase due to higher steam concentration explains the crystallization of LTA zeolite in BAx3-VPC45 (Fig. 3c).

The presence of no reactive glass amorphous material (Fig. 6), although in low amount, continues to limit the formation of zeolite A in BAx2-VPC45 (Fig. 3). The presence of sodalite in this sample (Fig. 3b) can be explained considering the inhomogeneous composition of geopolymeric materials determining local changes in its arrangement [54].

The treatment with vapor molecules at 60 and 90 °C controls the crystallization of sodalite in all the bauxite samples (Fig. 3). SEM pictures and EDX spectrum of this newly formed phase are shown in Fig. 7 and Fig. S4. The typical rose-like morphology of sodalite appears to be well defined at lower temperatures (60 °C), whereas it is hinted in BAx2 and BAx3 increasing the temperature of water bath up to 90 °C (Fig. 7). VPC process at higher temperature (60 and 90 °C) further increases the vapor saturation and, as consequence, the amount of water available for the crystallization process. The saturated steam conditions favor the bond breakage required for the rearrangement of geopolymer amorphous material [46], thus determining the synthesis of more stable crystalline structure of sodalite [27, 55, 56] in all the bauxite samples (Figs. 3 and 7). Based on these results, VPC process at higher temperature (60 and 90 °C) can be approximate to a hydrothermal process. This is in accordance with the hypothesis of Dimitrov et al. [48] describing VPC method as an intermediate mechanism between solid-state transformation and hydrothermal synthesis.

The role of water concentration and form generated by steam in controlling morphology of zeolite crystals is confirmed by the experiments carried out using *Device #b* and BAx2 sample. XRD patterns in Fig. 8 show the weak presence of LTA in BAx2-VPC35 and the increasing amount of sodalite in all the other samples. However, although X-ray profiles (Fig. 8) are comparable with the patterns of the same sample after VPC process using *Device #a* (Fig. 3b), SEM images show, instead, some differences. In fact, the pictures confirm the typical morphology of sodalite after VPC treatments at 45, 60 and 90 °C using *Device #b*, but the newly formed crystals are smaller and well separated (Fig. 9a', b', c') compared to the zeolite morphology characterizing the same BAx2 after VPC treatments with *Device #a* (Fig. 9a, b,

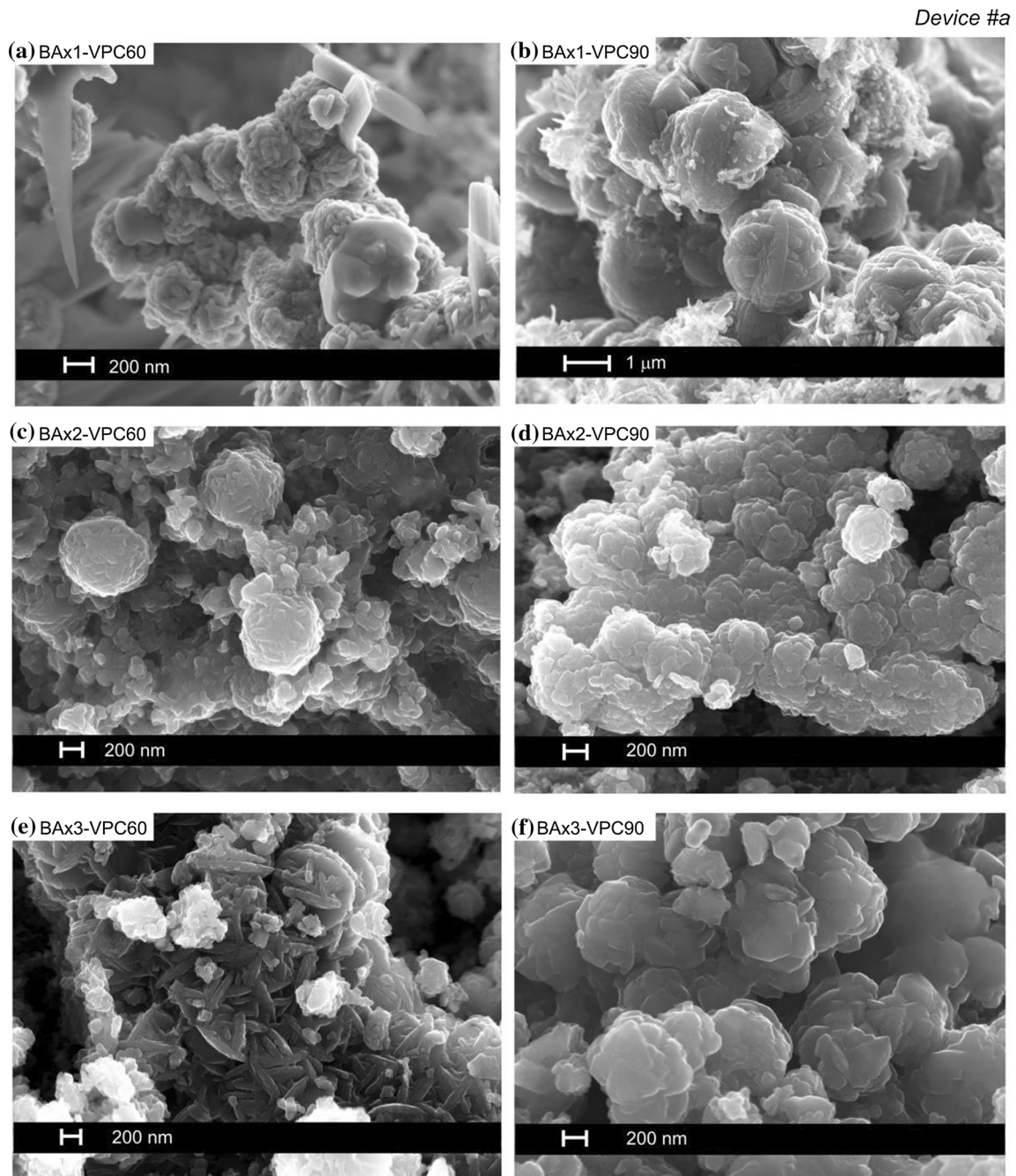
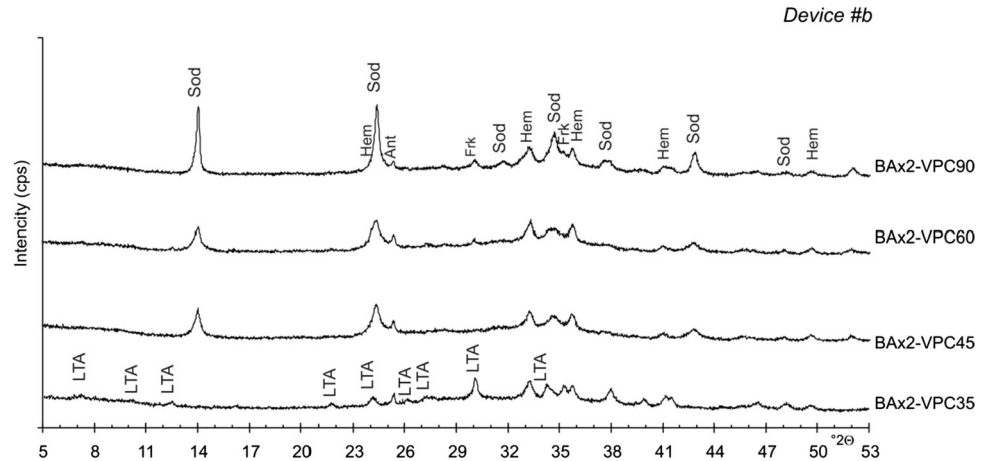


Figure 7 SEM images of: **a** BAX1 after VPC at 60 °C; **b** BAX1 after VPC at 90 °C; **c** BAX2 after VPC at 60 °C; **d** BAX2 after VPC at 90 °C; **e** BAX3 after VPC at 60 °C; **f** BAX3 after VPC at 90 °C using *Device #a*.

Figure 8 XRD patterns of BAx2 after VPC process at different temperatures using *Device #b*. LTA = zeolite A; Sod = sodalite; Frk = franklinite; Hem = hematite.



c). This indicates that the interface between raw materials and support in *Device #b* plays a key role in initiating crystallization improving the contact of raw material with water vapor molecules.

Conclusions

The experiments performed in this work indicate that natural inexpensive raw materials such as bauxites can be used to form zeolite by vapor crystallization process. The $\text{SiO}_2/\text{Al}_2\text{O}_3$ ratio, the competitive presence of geopolymers *vs* glass in amorphous materials and the general lower amount of water molecules, control the synthesis of zeolite with LTA topology during VPC at low temperature (35 and 45 °C). The larger amount of water by vapor crystallization treatment at higher temperature (60 and 90 °C) determines, instead, the formation of more stable sodalite with typical well-defined rose-like morphology by improving geopolymers crystallization. The role

of higher concentration of water vapor in type and morphology of zeolite formed is confirmed by the test carried out using *Device #b*. This device guarantees a complete immersion of the raw materials in steam, thus favoring the larger transformation geopolymer amorphous materials and the following synthesis of smaller and well-defined sodalite crystals. According to Chen and Huang [37] classification, the processes used to form zeolite with both *Device #a* and *Device #b* mainly at higher temperatures could be approximated to modified SAC and VPT methods, respectively.

Besides the mechanisms determining the type of zeolite crystallization, which certainly need more in-depth analysis, the results shown in this paper indicate that the vapor phase crystallization process represents a green and economic method to form zeolite reducing the amount of water and, most important think, generating no liquid waste generally produced by conventional hydrothermal method.

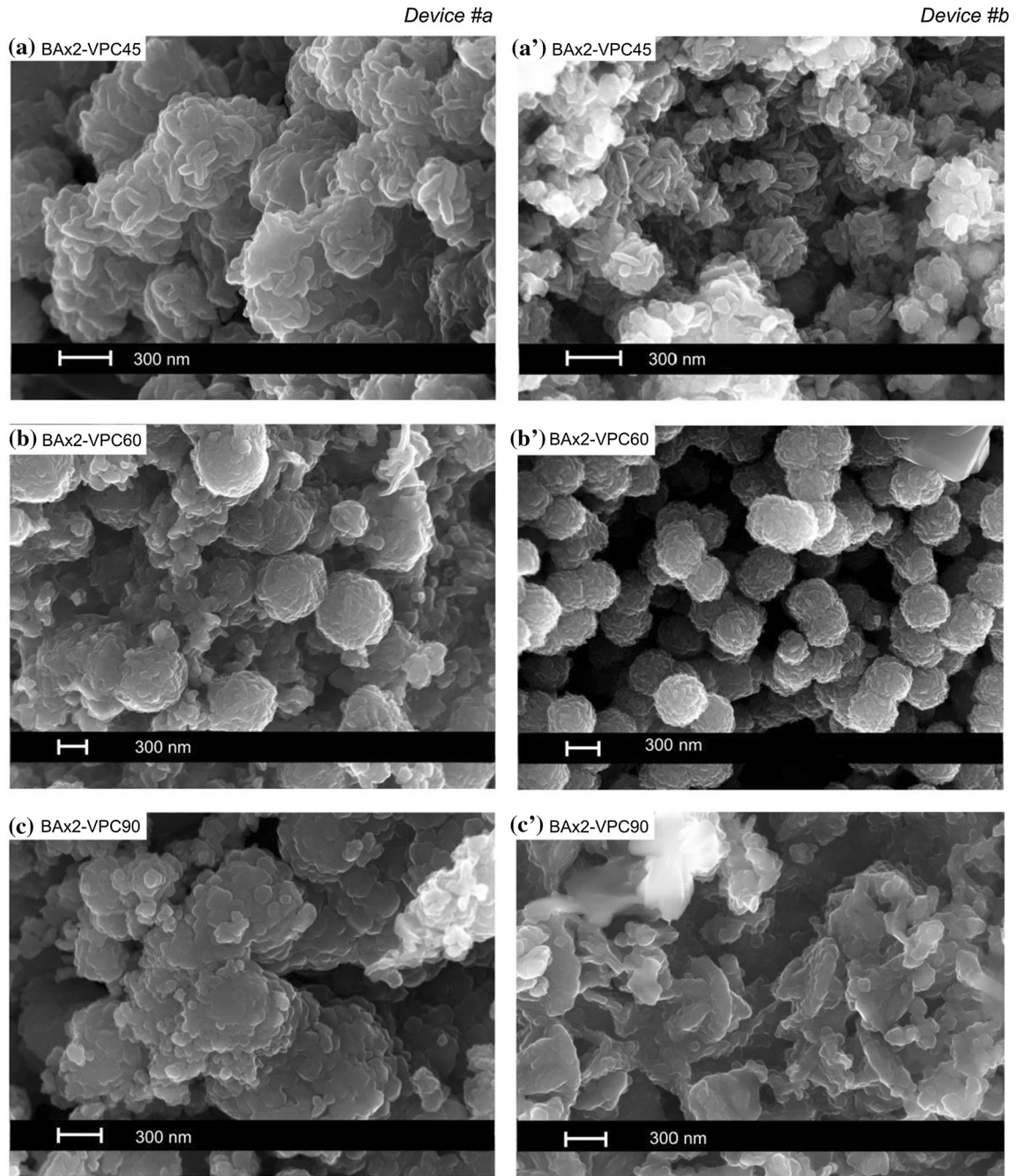


Figure 9 SEM images of BAx2 sample after VPC process at 45, 60 and 90 °C using *Device #a*, on the left and *Device #b*, on the right.

Declarations

Conflict of interest The authors declare that they have no conflict of interest.

Open Access This article is licensed under a Creative Commons Attribution 4.0 International License, which permits use, sharing, adaptation, distribution and reproduction in any medium or format, as long as you give appropriate credit to the original author(s) and the source, provide a link to the Creative Commons licence, and indicate if changes were made. The images or other third party material in this article are included in the article's Creative Commons licence, unless indicated otherwise in a credit line to the material. If material is not included in the article's Creative Commons licence and your intended use is not permitted by statutory regulation or exceeds the permitted use, you will need to obtain permission directly from the copyright holder. To view a copy of this licence, visit <http://creativecommons.org/licenses/by/4.0/>.

Supplementary Information: The online version contains supplementary material available at <http://doi.org/10.1007/s10853-022-07671-1>.

References

- [1] Agosta F, Manniello C, Cavalcante F, Belviso C, Prosser G (2021) Late cretaceous transtensional faulting of the Apulian platform. *Italy Mar Pet Geol* 127:104889
- [2] Bardossy G, Boni M, Dall'Aglia M, D'Argenio B, Panto G (1977) Bauxites of peninsular Italy: composition, origin and geotectonic significance. *Gebr Borntraeger* 15:
- [3] Gu J, Huang Z, Fan H, Jin Z, Yan Z, Zhang J (2013) Mineralogy, geochemistry, and genesis of the laterite bauxite deposits in the Wuchuan-Zheng'an-Daozhen area, Northern Guizhou Province, China. *J Geochem Explor* 130:44–59
- [4] Choi YS, Lee MS, Oh SH (2002) Manufacturing method of zeolite 4A using bauxite. *KR Patent 094527-A; 415941-B*
- [5] Choi YS, Lee MS, Oh SH (2004) Method for preparing zeolite. *KR Patent 028246-A; 491091-B*
- [6] Yan CJ, Han LX, Mei J, Yu HJ, Jiang L, Li WW, Xiao GQ, Hai SJ (2007) Process for producing 4A zeolite molecular sieve by temperature calcination. *CN Patent CN101172619-A*
- [7] Zhu YL, Chang ZH, Pang J, Xiong CJ (2011) Synthesis of Zeolite 4A from Kaolin and Bauxite by Alkaline fusion at low temperature. *Mat Sci Forum* 685:298–306
- [8] Kwakye-Awuah B, Sefa-Ntiri B, Von-Kiti E, Nkrumah I, Williams C (2019) Adsorptive removal of iron and manganese from groundwater samples in Ghana by Zeolite Y Synthesized from Bauxite and Kaolin. *Water* 11:1912–1931
- [9] Zhang Q, You W, Ma Y, Wang S (2020) Rice husk assisted like-dry-gel synthesis of FeSAPO-44 molecular sieve from natural bauxite. *J Solid State Chem* 291:121662
- [10] Wang C, Zhou J, Wang Y, Yang M, Lia Y, Meng C (2013) Synthesis of zeolite X from low-grade bauxite. *J Chem Technol Biotechnol* 88:1350–1357
- [11] Liu L, Du T, Li G, Yanga F, Che S (2014) Using one waste to tackle another: Preparation of a CO₂ capture material zeolite X from laterite residue and bauxite. *J Hazard Mater* 278:551–558
- [12] Qiang Z, Shen X, Guo M, Cheng F, Zhang M (2019) A simple hydrothermal synthesis of zeolite X from bauxite tailings for highly efficient adsorbing CO₂ at room temperature. *Microporous Mesoporous Mat* 287:77–84
- [13] Belviso C, Piancastelli A, Sturini M, Belviso S (2020) Synthesis of composite zeolite-layered double hydroxides using ultrasonic neutralized red mud. *Microporous Mesoporous Mat* 299:110108
- [14] Ma D, Wang Z, Guo M, Zhang M, Liu J (2014) Feasible conversion of solid waste bauxite tailings into highly crystalline 4A zeolite with valuable application. *Waste Manage* 34:2365–2372
- [15] Belviso C, Cannas C, Pinna N, Cavalcante F, Lettino A, Lotti P, Gatta GD (2020) Effect of red mud added to zeolite LTA synthesis: Where is Fe in the newly-formed material? *Microporous Mesoporous Mat* 298:1100583
- [16] Xie W, Zhou F, Bi X, Chen D, Li J, Sun S, Liu J, Chen X (2018) Accelerated crystallization of magnetic 4A-zeolite synthesized from red mud for application in removal of mixed heavy metal ions. *J Hazard Mater* 358:441–449
- [17] Belviso C, Kharchenko A, Agostinelli E, Cavalcante F, Peddis D, Varvaro G, Yaacoub N, Mintova S (2018) Red mud as aluminium source for the synthesis of magnetic zeolite. *Microporous Mesoporous Mat* 270:24–29
- [18] Cheng Y, Xu L, Jiang Z, Liu C, Zhang Q, Zou Y, Chen Y, Li J, Liu X (2021) Feasible low-cost conversion of red mud into magnetically separated and recycled hybrid SrFe₁₂O₁₉@-NaP1 zeolite as a novel wastewater adsorbent. *Chem Eng J* 417:128090
- [19] Belviso C, Agostinelli E, Belviso S, Cavalcante F, Pascucci S, Peddis D, Varvaro G, Fiore S (2015) Synthesis of magnetic zeolite at low temperature using a waste material

- mixture: fly ash and red mud. *Microporous Mesoporous Mat* 202:208–216
- [20] Belviso C, Abdolrahimi M, Peddis D, Gagliano E, Sgroi M, Lettino A, Roccaro P, Vagliasindi FGA, Falciglia PP, Di Bella G, Giustra MG, Cavalcante F (2021) Synthesis of zeolite from volcanic ash: characterization and application for cesium removal. *Microporous Mesoporous Mat* 319:111045
- [21] Garcia G, Cardenas E, Cabrera S, Hedlund J, Mouzon J (2016) Synthesis of zeolite Y from diatomite as silica source. *Microporous Mesoporous Mat* 219:29–37
- [22] Belviso C, Peddis D, Varvaro G, Abdolrahimi M, Reverberi AP, Cavalcante F (2020) Obsidian as raw material for eco-friendly synthesis of magnetic zeolite. *Materials* 13:4633
- [23] Tan W, Yap S, Matsumoto A, Othman R, Yeoh F (2011) Synthesis and characterization of zeolites NaA and NaY from rice husk ash. *Adsorption* 17:863–868
- [24] Belviso C, Cavalcante F, Niceforo G, Lettino A (2017) Sodalite, faujasite and A-type zeolite from 2:1 dioctahedral and 2:1:1 trioctahedral clay minerals. A singular review of synthesis methods through laboratory trials at a low incubation temperature. *Powder Technol* 320:483–497
- [25] Karami D, Rohani S (2009) Synthesis of pure zeolite Y using soluble silicate, a two-level factorial experimental design. *Chem Eng Process* 48:1288–1292
- [26] Saada MA, Soulard M, Patarin RC, Regis RC (2009) Synthesis of zeolite materials from asbestos wastes: an economical approach. *Microporous Mesoporous Mat* 122:275–282
- [27] Belviso C, Lettino A, Cavalcante F (2018) Influence of synthesis method on LTA time dependent stability. *Molecules* 23:2122–2130
- [28] Song H, Wan X, Sun X (2013) Preparation of Agy zeolites using microwave irradiation and study on their adsorptive desulphurisation performance. *Can J Chem Eng* 91:915–923
- [29] Belviso C (2016) EMT-type zeolite synthesized from obsidian. *Microporous Mesoporous Mat* 226:325–330
- [30] Belviso S, Cavalcante F, Lettino A, Ragone P, Belviso C (2016) Fly ash as raw material for the synthesis of zeolite-encapsulated porphyrazine and metallo porphyrazine tetrapyrrolic macrocycles. *Microporous Mesoporous Mat* 236:228–234
- [31] Larlus O, Mintova S, Bein T (2006) Environmental syntheses of nanosized zeolites with high yield and monomodal particle size distribution. *Microporous Mesoporous Mat* 96:405–412
- [32] Bukhari SS, Behin J, Kazemian H, Rohani S (2015) Conversion of coal fly ash to zeolite utilizing microwave and ultrasound energies: A review. *Fuel* 140:250–266
- [33] Belviso C (2018) Ultrasonic vs hydrothermal method: Different approaches to convert fly ash into zeolite. How they affect the stability of synthetic products over time? *Ultrason Sonochem* 43:9–14
- [34] Xie B, Zhang H, Yang C, Liu S, Ren L, Zhang L, Meng X, Yilmaz B, Mullerc U, Xiao F-S (2011) Seed-directed synthesis of zeolites with enhanced performance in the absence of organic templates. *Chem Commun* 47:3945–3947
- [35] Belviso C, Cavalcante F, Ragone P, Fiore S (2010) Immobilization of Ni by synthesising zeolite at low temperatures in a polluted soil. *Chemosphere* 78:1172–1176
- [36] Li Y, Yang W (2008) Microwave synthesis of zeolite membranes: A review. *J Membr Sci* 316:3–17
- [37] Chen B, Huang Y (2011) Formation of microporous material AlPO₄-18 under dry-gel conversion conditions. *Microporous Mesoporous Mat* 143:14–21
- [38] Matsukata M, Ogura M, Osaki T, Rao PRHP, Nomura M, Kikuchi E (1999) Conversion of dry-gel to micropores crystals in gas phase. *Top Catal* 9:77–92
- [39] Nishiyama N, Matsufuji T, Ueyama K, Matsukata M (1997) FER membrane synthesized by a vapor-phase transport method: its structure and separation characteristics. *Micropor Mater* 12:293–303
- [40] Nishiyama N, Ueyama K, Matsukata M (1995) A defect-free mordenite membrane synthesized by vapour-phase transport method. *J Chem Soc Chem Commun* 1967–1968.
- [41] Arnold A, Steuernagel S, Hunger M, Weitkamp J (2003) Insight into the dry-gel synthesis of gallium-rich zeolite [Ga]Beta. *Microporous Mesoporous Mat* 62:97–106
- [42] Mohammadparast F, Halladj R, Askari S (2018) The synthesis of nano-sized ZSM-5 zeolite by dry gel conversion method and investigating the effects of experimental parameters by Taguchi experimental design. *J Exp Nanosci* 13:160–173
- [43] Xu W, Dong J, Li J, Li J, Wu F (1990) A novel method for the preparation of zeolite ZSM-5. *Chem. Soc Chem Commun* 10:755–756
- [44] Kim M, Li H, Davis ME (1993) Synthesis of zeolites by water-organic vapor-phase transport. *Microporous Mater* 1:191–200
- [45] Matsukata M, Nishiyama N, Ueyama K (1996) Crystallization of FER and MFI zeolites by a vapor-phase transport method. *Microporous Mater* 7:109–117
- [46] Thoma SG, Neno TM (2000) Vapor phase transport synthesis of zeolites from sol-gel precursors. *Microporous Mesoporous Mat* 41:295–305
- [47] Cheng J, Pei S, Yue B, Qian L, He C, Zhou Y, He H (2008) Synthesis and characterization of hollow zeolite microspheres with a mesoporous shell by O/W/O emulsion and

- vapor-phase transport method. *Microporous Mesoporous Mat* 115:383–388
- [48] Dimitrov L, Valtechev V, Nihtianova D, Kalvachev Y (2011) Submicrometer zeolite A crystals formation: low-temperature crystallization versus vapor phase gel transformation. *Cryst Growth Des* 11:4958–4962
- [49] Larson, A.C., Von Dreele R.B. (2000) General structure analysis system (GSAS); Los Alamos National Laboratory, Los Alamos, 86–748
- [50] Krumm S (1999) The Erlangen geological and mineralogical software collection. *Comput Geosci* 25:489–499
- [51] Belviso C, Cavalcante F, Huertas FJ, Lettino A, Ragone P, Fiore S (2012) The crystallisation of zeolite (X- and A-type) from fly ash at 25 C in artificial sea water. *Microporous Mesoporous Mat* 162:115–121
- [52] Fernandez-Jimenez A, Palomo A (2005) Mid-infrared spectroscopic studies of alkali-activated fly ash structure. *Microporous Mesoporous Mat* 86:207–214
- [53] Alvarez-Ayuso E, Querol X, Plana F, Alastuey A, Moreno N, Izquierdo M, Font O, Moreno T, Diez S, Vázquez E, Barr M, (2008) Environmental, physical and structural characterisation of geopolymer matrixes synthesised from coal (co-) combustion fly ashes. *J Hazard Mater* 154:175–183
- [54] Belviso C, Giannossa LC, Huertas FJ, Lettino A, Mangone A, Fiore S (2015) Synthesis of zeolites at low temperatures in fly ash-kaolinite mixtures. *Microporous Mesoporous Mat* 212:35–47
- [55] Walton RI, Millange F, O'Hare D, Davies AT, Sankar G (2001) Catlow CRA (2001) An in situ energy-dispersive x-ray diffraction study of the hydrothermal crystallization of zeolite A. 1. Influence of reaction conditions and transformation into sodalite. *J Phys Chem B* 105:83–90
- [56] Greer H, Wheatley PS, Ashbrook SE, Morris RE, Zhou W (2009) Early stage reversed crystal growth of zeolite a and its phase transformation to sodalite. *J Am Chem Soc* 131:17986–17992

Publisher's Note Springer Nature remains neutral with regard to jurisdictional claims in published maps and institutional affiliations.